Advances in Nano Research, *Vol. 11, No. 4 (2021) 393-403*
https://doi.org/10.12989/anr.2021.11.4.393

Analytical and mathematical simulation for nonlinear stability of scale-dependent magneto-electro-elastic system

Bin Li*[1], Xiaojia Xu[1], Zhigang Hu[1], Yuzuo Liu[1,2], Menghui Qi[2] and Zengquan Zheng[2]

[1]*School of Mechanical Engineering, Wuhan Polytechnic University, Wuhan 430023 Hubei, China*
[2]*Hubei Key Laboratory of Theory and Application of Advanced Materials Mechanics, Wuhan University of Technology 430070 Hubei, China*

(*Received March 20, 2021, Revised August 12, 2021, Accepted August 12, 2021*)

Abstract. By using differential quadrature method (DQM), a numerical investigation was provided for nonlinear stability behavior of magneto-electro-elastic (MEE) cylindrical shells at microscale. It is assumed that the cylindrical shell has been subjected to compressive loads leading to buckling phenomena in geometrically nonlinear regime. The non-uniformity of strain field has been inserted in the formulation for considering the microscale effects. The material properties of the shell are considered to be inhomogeneous with graded distribution. After solving the governing equations using DQM, it is realized that if the nanoscale shell is subjected to electrical and magnetic fields, the post-buckling path may be changed with the value of electrical voltage and magnetic potential. Also, strain gradient effects have remarkable influence on post-buckling curves and critical voltages.

Keywords: classic shell theory; magneto-electro-elastic materials; nonlinear stability; smart material; strain gradient theory

1. Introduction

Presenting supreme mechanical performance within electric and magnetic environments, magneto-electrical-elastic (MEE) materials can be introduced as a sort of ingenious materials with excellent applications in sensing devices, ingenious systems and structures (Pan 2001). Subjecting to an external mechanical force, such smart materials are able to represent electro-magnetic field sensing. Also, subjecting to an electro-magnetic field, these materials experience mechanical deformation (Ramirez *et al*. 2006). As an instance, $BaTiO_3$ and $CoFe_2O_4$ may be combined to each other in order to produce composites of MEE material. Based on the percentages of these two materials, it will be possible to describe any material property of the composites including elastic modulus and piezo-magnetic constants. However, the particles of these materials are not directly combined and it is possible to provide a graded distribution of materials. Actually, functionally graded (FG) materials can be produced with the gradation the two materials (Chikh *et al*. 2016, Sayyad and Ghugal 2018). Mathematical description of FG materials can be done using a power-law function. In fact, a FG-MEE material might be created and described with specific properties which are varying from $BaTiO_3$ to $CoFe_2O_4$ or contrariwise (Barati and Zenkour 2018).

Recently, many papers have been devoted to material and structural characterization (Chen *et al*. 2020, Dai *et al*. 2020, 2021a, b, Fang *et al*. 2020, Kovalnogov *et al*. 2020, Li *et al*. 2021, Medvedev *et al*. 2020, 2021a, b, Qiao *et al*. 2021, Simos *et al*. 2020, 2021, Sun *et al*. 2021, Tan *et al*. 2021, Xu and Nieto-Vesperinas 2019, Yan *et al*. 2020, Zhang and Ou 2015, Zhang and Zhang 2021a, b, Zhao *et al*. 2020a, b, Zhu *et al*. 2020). Mathematical description of nano-sized structural components such as shells can be performed by utilizing several new elasticity theories which differ from classical elasticity theory (Ebrahimi and Barati 2019a, b, c, Fenjan *et al*. 2021, Ahmed *et al*. 2020a, b, c, Muhammad *et al*. 2019). Some of these theories are known as nonlocal theory and strain gradient theory which have small-scale parameters in order to explain size-dependent behavior of nano-sized structures (Eltaher *et al*. 2016, Barretta *et al*. 2016, Heydarpour and Malekzadeh 2019). Based on previous researches, a structural stiffness increment has been provided by strain gradient influence. Also, a structural stiffness reduction has been reported based on nonlocal elasticity theory of Eringen (1983). This stiffness reduction is observed for nanoshells leading to lower vibration frequencies and buckling loads compared to macro-size shells (Zeighampour *et al*. 2018). Taking into account the effect of nonlocal elasticity, static/dynamic properties of nano-sized magneto-electro-elastic structures have been investigated by various authors (Ke and Wang 2014, Farajpour *et al*. 2016, Ke *et al*. 2014, Waksmanski and Pan 2017).

Simultaneous effects of nonlocal and strain gradient theory can be captured via a unified theory named nonlocal strain gradient theory (NSGT). As proved by molecular dynamic simulations, the two parameters play an important role in mechanical behaviors of nanostructures (Mehralian *et al*. 2017a, b). In recent years, many authors tried to examine static and dynamical responses of nano-structural components in the framework of NSGT. NSGT modeling

*Corresponding author, Ph.D.,
E-mail: lb420@whpu.edu.cn

ISSN: 2287-237X (Print), 2287-2388 (Online)

and buckling analysis of a nanobeam based on classic beam theory is carried out by Li and Hu (2015). Utilizing a shear deformation beam theory and NSGT, Lu *et al*. (2017) researched vibrational frequencies of a beam with nano-dimension. Based on NSGT formulation, examination of nonlinear bending/vibration characteristics of FG nanobeams have been accomplished by Li and Hu (2016). In another study, closed-forms of bending solution and vibration solution for NAGT-modeled FG nanobeams have been introduces by Simsek (2019). Moreover, wave propagation characteristics of nanoshells possessing magneto-electro-elastic material of functionally graded type are researched by Ma *et al*. (2018). In another work, she *et al*. (2018) researched geometrically nonlinear deflections and frequency curves of a cylindrical nanoshell possessing FG properties in the context of NSGT. In the context of NSGT, Arefi *et al*. (2019) examined bending properties of nano-sized plate structures with bottom and top layers of magneto-electro-elastic material. By searching in the literature, it can be deduced that post-buckling behavior of FG-METE cylindrical nanoshell in the context of NSGT and taking into account geometric nonlinear effects is not explored yet.

By using differential quadrature method (DQM), a numerical investigation was provided for nonlinear stability behavior of magneto-electro-elastic (MEE) cylindrical shells at microscale. It is assumed that the cylindrical shell has been subjected to compressive loads leading to buckling phenomena in geometrically nonlinear regime. The non-uniformity of strain field has been inserted in the formulation for considering the microscale effects. The material properties of the shell are considered to be inhomogeneous with graded distribution. After solving the governing equations using DQM, it is realized that if the nanoscale shell is subjected to electrical and magnetic fields, the post-buckling path may be changed with the value of electrical voltage and magnetic potential. Also, strain gradient effects have remarkable influence on post-buckling curves.

2. Strain gradient micro-shell modeling

A scale parameter has been considered in strain gradient theory which is called strain gradient parameter (l). So, stress-strain relationship for strain gradient theory dependents on this parameter. By knowing that ∇^2 is Laplacian operator, the stress-strain relationship based on strain gradient theory may be written by (Ebrahimi *et al*. 2016):

$$\sigma_{ij} = C_{ijkl}[1 - l^2\nabla^2]\varepsilon_{kl} \tag{1}$$

Here, C_{ijkl} defines the material properties; σ_{ij} and ε_{kl} are the stress and strain components. By assuming l = 0, the stress-strain relation based on classical elasticity theory will be achieved (Aydogdu *et al*. 2018, Uzun and Civalek 2019).

$$\sigma_{ij}^{(0)} = C_{ijkl}\varepsilon_{kl} \tag{2}$$

3. Shells made of FG-MEE materials

Power-law function is known as an effectual model for

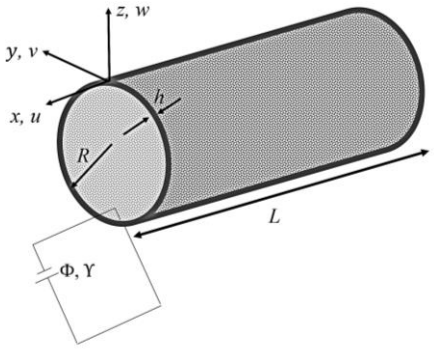

Fig. 1 Configuration of MEE cylindrical microshell

characterizing a functionally graded material. This function is able to describe material distribution in transverse direction. So, it is possible to express each material property (P_f) such as piezo-magnetic and elastic properties in such a way that they vary from top surface (P_t) to bottom surface (P_b) based on following relation:

$$P_f(z) = (P_t - P_b)(\frac{z}{h} + \frac{1}{2})^p + P_b \tag{3}$$

Material gradient index (p) is able to characterize material dispersions along thickness direction of the nanoshell. Here, h is microshell thickness.

There are different theories for modeling of beams, plates and shells (Barati and Shahverdi 2021, Mirjavadi *et al*. 2020a, b, c, d, e, f, g, h, Shariati *et al*. 2020a, b). In order to establish nonlinear formulation for post-buckling of the microshell, traditional or classic shell theory has been employed in this research. Accordingly, the displacements of microshell (u_1, u_2, u_3) might be expressed based upon longitudinal (u), circumferential (v) and transverse (w) field components as:

$$u_1(x,y,z) = u(x,y) - z\frac{\partial w}{\partial x}(x,y) \tag{4}$$

$$u_2(x,y,z) = v(x,y) - \frac{z}{R}\frac{\partial w}{\partial y}(x,y) \tag{5}$$

$$u_3(x,y,z) = w(x,y) \tag{6}$$

The strain field of microshells incorporating the geometrical nonlinearity is:

$$\begin{aligned}
\varepsilon_{xx} &= \frac{\partial u}{\partial x} - z\frac{\partial^2 w}{\partial x^2} + \frac{1}{2}\left(\frac{\partial w}{\partial x}\right)^2 \\
\varepsilon_{yy} &= \frac{\partial v}{\partial y} - \frac{w}{R} - z\frac{\partial^2 w}{\partial y^2} + \frac{1}{2}\left(\frac{\partial w}{\partial y}\right)^2 \\
\gamma_{xy} &= \frac{\partial u}{\partial y} + \frac{\partial v}{\partial x} - 2z\frac{\partial^2 w}{\partial x \partial y} + \frac{\partial w}{\partial x}\frac{\partial w}{\partial y}
\end{aligned} \tag{7}$$

Bearing in mind that MEE microshell is exposed to electrical-magnetic field having electric (Φ) and magnetic potentials (Υ), it is possible to express the potentials as follows based on electric voltage (V) and magnetic intensity (Ω):

$$\Phi(x,y,z) = -\cos(\xi z)\phi(x,y) + \frac{2z}{h}V \tag{8}$$

$$\Upsilon(x,y,z) = -\cos(\xi z)\gamma(x,y) + \frac{2z}{h}\Omega \tag{9}$$

where $\xi = \pi/h$. Determining all gradients of electrical-magnetic potentials leads to the electric field (E_x, E_θ, E_z) and magnet field components (H_x, H_θ, H_z) in below form:

$$E_x = -\Phi_{,x} = \cos(\xi z)\frac{\partial \phi}{\partial x}, \tag{10}$$

$$E_y = -\Phi_{,y} = \cos(\xi z)\frac{\partial \phi}{\partial y}, \tag{11}$$

$$E_z = -\Phi_{,z} = -\xi \sin(\xi z)\phi - \frac{2V}{h} \tag{12}$$

$$H_x = -\Upsilon_{,x} = \cos(\xi z)\frac{\partial \gamma}{\partial x}, \tag{13}$$

$$H_y = -\Upsilon_{,y} = \cos(\xi z)\frac{\partial \gamma}{\partial y}, \tag{14}$$

$$H_z = -\Upsilon_{,z} = -\xi \sin(\xi z)\gamma - \frac{2\Omega}{h} \tag{15}$$

All components of stress field, electric environment displacement (D_x, D_y, D_z) and magnetic inductions (B_x, B_y, B_z) for a scale-dependent microshell within the framework of SGT might be introduced as:

$$\sigma_{xx} = (1 - l^2\nabla^2)[\tilde{C}_{11}\varepsilon_{xx} + \tilde{C}_{12}\varepsilon_{yy}] - \tilde{e}_{31}E_z - \tilde{q}_{31}H_z - \tilde{c}_{11}\tilde{\alpha}_1\Delta T \tag{16}$$

$$\sigma_{yy} = (1 - l^2\nabla^2)[\tilde{C}_{12}\varepsilon_{xx} + \tilde{C}_{11}\varepsilon_{yy}] - \tilde{e}_{31}E_z - \tilde{q}_{31}H_z - \tilde{c}_{11}\tilde{\alpha}_1\Delta T \tag{17}$$

$$\sigma_{xy} = (1 - l^2\nabla^2)\tilde{C}_{66}\gamma_{xy} \tag{18}$$

$$D_x = +\tilde{s}_{11}E_x + \tilde{d}_{11}H_x \tag{19}$$

$$D_y = +\tilde{s}_{11}E_y + \tilde{d}_{11}H_y \tag{20}$$

$$D_z = (1 - l^2\nabla^2)[\tilde{e}_{31}\varepsilon_{xx} + \tilde{e}_{31}\varepsilon_{yy}] + \tilde{s}_{33}E_z + \tilde{d}_{33}H_z \tag{21}$$

$$B_x = +\tilde{d}_{11}E_x + \tilde{\chi}_{11}H_x \tag{22}$$

$$B_y = +\tilde{d}_{11}E_y + \tilde{\chi}_{11}H_y \tag{23}$$

$$B_z = (1 - l^2\nabla^2)[\tilde{q}_{31}\varepsilon_{xx} + \tilde{q}_{31}\varepsilon_{yy}] + \tilde{d}_{33}E_z + \tilde{\chi}_{33}H_z \tag{24}$$

Elasto-piezo-magnetic material properties have been respectively represented by C_{ij}, e_{ij} and q_{ij}. Bearing in mind the plane stress conditions, each material property can be re-written as (Ke *et al*. 2014):

$$\begin{aligned}
&\tilde{C}_{11} = C_{11} - \frac{C_{13}^2}{C_{33}}, \quad \tilde{C}_{12} = C_{12} - \frac{C_{13}^2}{C_{33}},\\
&\tilde{C}_{66} = C_{66}, \quad \tilde{e}_{31} = e_{31} - \frac{C_{13}e_{33}}{c_{33}},\\
&\tilde{q}_{31} = q_{31} - \frac{C_{13}q_{33}}{C_{33}}, \quad \tilde{d}_{11} = \tilde{d}_{11},\\
&\tilde{d}_{33} = \tilde{d}_{33} + \frac{q_{33}e_{33}}{C_{33}}, \tilde{s}_{11} = s_{11}, \quad \tilde{s}_{33} = s_{33} + \frac{e_{33}^2}{C_{33}},\\
&\tilde{\chi}_{11} = \chi_{11}, \quad \tilde{\chi}_{33} = \chi_{33} + \frac{q_{33}^2}{C_{33}}, \quad \tilde{\alpha}_1 = \alpha_1 - \frac{c_{13}\alpha_3}{c_{33}}
\end{aligned} \tag{25}$$

If *U* denotes strain energy of the microshell and *V* is the work of external forces, it is possible to introduce Hamilton's rule using the below equation (Medani *et al*. 2017):

$$\int_0^t \delta(U - V)dt = 0 \tag{26}$$

where

$$\begin{aligned}
\delta U = \int_V (&\sigma_{xx}^{(0)}\delta\varepsilon_{xx} + \sigma_{xx}^{(1)}\delta\nabla\varepsilon_{xx} + \sigma_{yy}^{(0)}\delta\varepsilon_{yy}\\
&+\sigma_{yy}^{(1)}\delta\nabla\varepsilon_{yy} + \sigma_{xy}^{(0)}\delta\gamma_{xy} + \sigma_{xy}^{(1)}\delta\nabla\gamma_{xy}\\
&-D_x\delta E_x - D_y\delta E_y - D_z\delta E_z - B_x\delta H_x\\
&-B_y\delta H_y - B_z\delta H_z)dV
\end{aligned} \tag{27}$$

$$\delta V = \int_V (N_{x0}(\frac{\partial^2 w}{\partial x^2}) + N_{y0}\frac{\partial^2 w}{\partial y^2}))\delta w dV \tag{28}$$

Furthermore, the exerted forces are:

$$N_{x0} = N_{y0} = N^E + N^H + N^M \tag{29}$$

Exerted forces in longitudinal and lateral directions have become the sum of elastic loading (N^M), electrical loading (N^E), and magnetic loading (N^H) in such a way that:

$$\begin{aligned}
N^E &= -\int_{-h/2}^{h/2} \tilde{e}_{31}\frac{2V}{h}dz,\\
N^H &= -\int_{-h/2}^{h/2} \tilde{q}_{31}\frac{2\Omega}{h}dz
\end{aligned} \tag{30}$$

With the help of Eq. (26), the compilation of field variables leads to the subsequent governing equations of microshells:

$$\frac{\partial N_{xx}}{\partial x} + \frac{\partial N_{xy}}{\partial y} = 0 \tag{31}$$

$$\frac{\partial N_{xy}}{\partial x} + \frac{\partial N_{yy}}{\partial y} = 0 \tag{32}$$

$$\begin{aligned}
&\frac{\partial^2 M_{xx}}{\partial x^2} + 2\frac{\partial^2 M_{xy}}{\partial x \partial y} + \frac{\partial^2 M_{yy}}{\partial y^2} + \frac{N_{yy}}{R}\\
&+(N_{x0} + N_{xx})(\frac{\partial^2 w}{\partial x^2}) + (N_{y0} + N_{yy})(\frac{\partial^2 w}{\partial y^2})\\
&+2N_{xy}\frac{\partial^2 w}{\partial x \partial y} = 0
\end{aligned} \tag{33}$$

$$\int_{-h/2}^{h/2}\begin{pmatrix}cos(\xi z)\dfrac{\partial D_x}{\partial x}+cos(\xi z)\dfrac{\partial D_y}{\partial y}\\+\xi\, sin(\xi z)D_z\end{pmatrix}dz=0 \tag{34}$$

$$\int_{-h/2}^{h/2}\begin{pmatrix}cos(\xi z)\dfrac{\partial B_x}{\partial x}+cos(\xi z)\dfrac{\partial B_y}{\partial y}\\+\xi\, sin(\xi z)B_z\end{pmatrix}dz=0 \tag{35}$$

It should be clarified that N_{rs} and M_{rs} (rs=xx, xy, yy) express membrane loads and out-of-plane moments:

$$\begin{aligned}
N_{xx}&=\int_{-h/2}^{h/2}(\sigma_{xx}^{(0)}-\nabla\sigma_{xx}^{(1)})dz=N_{xx}^{(0)}-\nabla N_{xx}^{(1)}\\
N_{xy}&=\int_{-h/2}^{h/2}(\sigma_{xy}^{(0)}-\nabla\sigma_{xy}^{(1)})dz=N_{xy}^{(0)}-\nabla N_{xy}^{(1)}\\
N_{yy}&=\int_{-h/2}^{h/2}(\sigma_{yy}^{(0)}-\nabla\sigma_{yy}^{(1)})dz=N_{yy}^{(0)}-\nabla N_{yy}^{(1)}\\
M_{xx}&=\int_{-h/2}^{h/2}z(\sigma_{xx}^{(0)}-\nabla\sigma_{xx}^{(1)})dz=M_{x}^{b(0)}-\nabla M_{xx}^{b(1)}\\
M_{y}&=\int_{-h/2}^{h/2}z(\sigma_{yy}^{(0)}-\nabla\sigma_{yy}^{(1)})dz=M_{y}^{b(0)}-\nabla M_{y}^{b(1)}\\
M_{xy}&=\int_{-h/2}^{h/2}z(\sigma_{xy}^{(0)}-\nabla\sigma_{xy}^{(1)})dz=M_{xy}^{b(0)}-\nabla M_{xy}^{b(1)}
\end{aligned} \tag{36}$$

In above relations:

$$\begin{aligned}
N_{ij}^{(0)}&=\int_{-h/2}^{h/2}(\sigma_{ij}^{(0)})dz,\quad N_{ij}^{(1)}=\int_{-h/2}^{h/2}(\sigma_{ij}^{(1)})dz\\
M_{ij}^{(0)}&=\int_{-h/2}^{h/2}z(\sigma_{ij}^{(0)})dz,\quad M_{ij}^{(1)}=\int_{-h/2}^{h/2}z(\sigma_{ij}^{(1)})dz
\end{aligned} \tag{37}$$

In order to define classical and non-classical stresses, two symbols have been respectively employed as $^{(0)}$ and $^{(1)}$. With the help of Hamilton's rule, it is feasible to calculate electro-elastic BCs for MEE microshell taking into account n_x and n_y as cosines of orientation:

$$u=0, or N_{xx}n_x+N_{xy}n_y=0 \tag{38}$$

$$v=0, or N_{xy}n_x+N_{yy}n_y=0 \tag{39}$$

$$\begin{aligned}
&w=0, or n_x\left(\frac{\partial M_{xx}}{\partial x}+\frac{\partial M_{xy}}{\partial y}-N_{x0}\frac{\partial w}{\partial x}\right)\\
&+n_y\left(\frac{\partial M_{yy}}{\partial y}+\frac{\partial M_{xy}}{\partial x}-N_{y0}\frac{\partial w}{\partial y}\right)=0
\end{aligned} \tag{40}$$

$$\frac{\partial w}{\partial x}=0, or M_{xx}n_x+M_{xy}n_y=0 \tag{41}$$

$$\frac{\partial w}{\partial y}=0, or M_{xy}n_x+M_{yy}n_y=0 \tag{42}$$

$$\phi=0, or\int_{-h/2}^{h/2}\begin{pmatrix}cos(\xi z)D_xn_x\\+cos(\xi z)D_yn_y\end{pmatrix}dz=0 \tag{43}$$

$$\gamma=0, or\int_{-h/2}^{h/2}\begin{pmatrix}cos(\xi z)B_xn_x\\+cos(\xi z)B_yn_y\end{pmatrix}dz=0 \tag{44}$$

Determining the integrals represented in Eq.(36) results in the below relations for MEE microshells based on SGT as:

$$\begin{aligned}
N_{xx}&=(1-l^2\nabla^2)[A_{11}(\frac{\partial u}{\partial x}+\frac{1}{2}(\frac{\partial w}{\partial x})^2)-B_{11}\frac{\partial^2 w}{\partial x^2}\\
&+A_{12}(\frac{\partial v}{\partial y}-\frac{w}{R}+\frac{1}{2}(\frac{\partial w}{\partial y})^2)-B_{12}\frac{\partial^2 w}{\partial y^2})]+A_{31}^{e}\phi+A_{31}^{m}\gamma
\end{aligned} \tag{45}$$

$$\begin{aligned}
M_{xx}&=(1-l^2\nabla^2)[B_{11}(\frac{\partial u}{\partial x}+\frac{1}{2}(\frac{\partial w}{\partial x})^2)-D_{11}\frac{\partial^2 w}{\partial x^2}\\
&+B_{12}(\frac{\partial v}{\partial y}-\frac{w}{R}+\frac{1}{2}(\frac{\partial w}{\partial y})^2)-D_{12}\frac{\partial^2 w}{\partial y^2}]+E_{31}^{e}\phi+E_{31}^{m}\gamma
\end{aligned} \tag{46}$$

$$\begin{aligned}
N_{yy}&=(1-l^2\nabla^2)[A_{12}(\frac{\partial u}{\partial x}+\frac{1}{2}(\frac{\partial w}{\partial x})^2)-B_{12}\frac{\partial^2 w}{\partial x^2}\\
&+A_{11}(\frac{\partial v}{\partial y}-\frac{w}{R}+\frac{1}{2}(\frac{\partial w}{\partial y})^2)-B_{11}\frac{\partial^2 w}{\partial y^2}]+A_{31}^{e}\phi+A_{31}^{m}\gamma
\end{aligned} \tag{47}$$

$$\begin{aligned}
M_{yy}&=(1-l^2\nabla^2)[B_{12}(\frac{\partial u}{\partial x}+\frac{1}{2}(\frac{\partial w}{\partial x})^2)-D_{12}\frac{\partial^2 w}{\partial x^2}\\
&+B_{11}(\frac{\partial v}{\partial y}-\frac{w}{R}+\frac{1}{2}(\frac{\partial w}{\partial y})^2)-D_{11}\frac{\partial^2 w}{\partial y^2}]+E_{31}^{e}\phi+E_{31}^{m}\gamma
\end{aligned} \tag{48}$$

$$\begin{aligned}
N_{xy}&=(1-l^2\nabla^2)[A_{66}(\frac{\partial u}{\partial y}+\frac{\partial v}{\partial x}+\frac{\partial w}{\partial x}\frac{\partial w}{\partial y})\\
&-2B_{66}\frac{\partial^2 w}{\partial x\partial y}]
\end{aligned} \tag{49}$$

$$\begin{aligned}
M_{xy}&=(1-l^2\nabla^2)[B_{66}(\frac{\partial u}{\partial y}+\frac{\partial v}{\partial x}+\frac{\partial w}{\partial x}\frac{\partial w}{\partial y})\\
&-2D_{66}\frac{\partial^2 w}{\partial x\partial y}]
\end{aligned} \tag{50}$$

$$\int_{-\hbar/2}^{\hbar/2}D_x\, cos(\xi z)dz=+F_{11}^{e}\frac{\partial\phi}{\partial x}+F_{11}^{m}\frac{\partial\gamma}{\partial x} \tag{51}$$

$$\int_{-h/2}^{h/2}D_y\, cos(\xi z)dz=+F_{22}^{e}\frac{\partial\phi}{\partial y}+F_{22}^{m}\frac{\partial\gamma}{\partial y} \tag{52}$$

$$\begin{aligned}
\int_{-h/2}^{h/2}D_z\xi\, sin(\xi z)dz&=A_{31}^{e}(\frac{\partial u}{\partial x}+\frac{1}{2}(\frac{\partial w}{\partial x})^2)\\
&+A_{31}^{e}(\frac{\partial v}{\partial y}-\frac{w}{R}+\frac{1}{2}(\frac{\partial w}{\partial y})^2)-E_{31}^{e}(\frac{\partial^2 w}{\partial x^2}+\frac{\partial^2 w}{\partial y^2})\\
&-F_{33}^{e}\phi-F_{33}^{m}\gamma
\end{aligned} \tag{53}$$

$$\int_{-\hbar/2}^{\hbar/2}B_x\, cos(\xi z)dz=+F_{11}^{m}\frac{\partial\phi}{\partial x}+X_{11}^{m}\frac{\partial\gamma}{\partial x} \tag{54}$$

$$\int_{-h/2}^{h/2}B_y\, cos(\xi z)dz=+F_{22}^{m}\frac{\partial\phi}{\partial y}+X_{22}^{m}\frac{\partial\gamma}{\partial y} \tag{55}$$

$$\begin{aligned}
\int_{-h/2}^{h/2}B_z\xi\, sin(\xi z)dz&=A_{31}^{m}(\frac{\partial u}{\partial x}+\frac{1}{2}(\frac{\partial w}{\partial x})^2)\\
&+A_{31}^{m}(\frac{\partial v}{\partial y}-\frac{w}{R}+\frac{1}{2}(\frac{\partial w}{\partial y})^2)\\
&-E_{31}^{m}(\frac{\partial^2 w}{\partial x^2}+\frac{\partial^2 w}{\partial y^2})-F_{33}^{m}\phi-X_{33}^{m}\gamma
\end{aligned} \tag{56}$$

in which

$$\{A_{11}, B_{11}, D_{11}\} = \int_{-\hbar/2}^{\hbar/2} \tilde{C}_{11}\{1, z, z^2\}dz, \tag{57}$$

$$\{A_{12}, B_{12}, D_{12}\} = \int_{-\hbar/2}^{\hbar/2} \tilde{C}_{12}\{1, z, z^2\}dz, \tag{58}$$

$$\{A_{66}, B_{66}, D_{66}\} = \int_{-h/2}^{h/2} \tilde{C}_{66}\{1, z, z^2\}dz, \tag{59}$$

$$\{A_{31}^e, E_{31}^e\} = \int_{-h/2}^{h/2} \tilde{e}_{31}\xi\, sin(\xi z)\{1, z\}\, dz \tag{60}$$

$$\{A_{31}^m, E_{31}^m\} = \int_{-h/2}^{h/2} \tilde{q}_{31}\xi\, sin(\xi z)\{1, z\}\, dz \tag{61}$$

$$\{F_{11}^e, F_{22}^e, F_{33}^e\} = \int_{-h/2}^{h/2} \{\tilde{s}_{11}\, cos^2(\xi z), \tilde{s}_{22}\, cos^2(\xi z), \tilde{s}_{33}\xi^2\, sin^2(\xi z)\}\, dz \tag{62}$$

$$\{F_{11}^m, F_{22}^m, F_{33}^m\} = \int_{-h/2}^{h/2} \{\tilde{d}_{11}\, cos^2(\xi z), \tilde{d}_{22}\, cos^2(\xi z), \tilde{d}_{33}\xi^2\, sin^2(\xi z)\}\, dz \tag{630}$$

$$\{X_{11}^m, X_{22}^m, X_{33}^m\} = \int_{-h/2}^{h/2} \{\tilde{\chi}_{11}\, cos^2(\xi z), \tilde{\chi}_{22}\, cos^2(\xi z), \tilde{\chi}_{33}\xi^2\, sin^2(\xi z)\}\, dz \tag{64}$$

The possible governing equations for MEE microshells induced by electro-magnetic environments incorporating strain gradient influence can be derived by placing Eqs. (45)-(56) into Eqs. (31)-(35) as:

$$\begin{aligned}
&(1-l^2\nabla^2)[A_{11}(\frac{\partial^2 u}{\partial x^2}+\frac{\partial^2 w}{\partial x^2}\frac{\partial w}{\partial x}) - B_{11}\frac{\partial^3 w}{\partial x^3}\\
&+A_{12}(\frac{\partial^2 v}{\partial x\partial y}-\frac{1}{R}\frac{\partial w}{\partial x}+\frac{\partial^2 w}{\partial x\partial y}\frac{\partial w}{\partial y}) - B_{12}\frac{\partial^3 w}{\partial x\partial y^2}\\
&+A_{66}(\frac{\partial^2 u}{\partial y^2}+\frac{\partial^2 v}{\partial x\partial y}+\frac{\partial^2 w}{\partial x\partial y}\frac{\partial w}{\partial y}+\frac{\partial w}{\partial x}\frac{\partial^2 w}{\partial y^2})\\
&-2B_{66}\frac{\partial^3 w}{\partial x\partial y^2}] + A_{31}^e\frac{\partial \phi}{\partial x}+A_{31}^m\frac{\partial \gamma}{\partial x} = 0
\end{aligned} \tag{65}$$

$$\begin{aligned}
&(1-l^2\nabla^2)[A_{66}(\frac{\partial^2 u}{\partial x\partial y}+\frac{\partial^2 v}{\partial x^2}+\frac{\partial^2 w}{\partial x^2}\frac{\partial w}{\partial y}\\
&+\frac{\partial w}{\partial x}\frac{\partial^2 w}{\partial x\partial y}) - 2B_{66}\frac{\partial^3 w}{\partial x^2\partial y}\\
&+A_{12}(\frac{\partial^2 u}{\partial x\partial y}+\frac{\partial w}{\partial x}\frac{\partial^2 w}{\partial x\partial y}) - B_{12}\frac{\partial^3 w}{\partial x^2\partial y}\\
&+A_{11}(\frac{\partial^2 v}{\partial y^2}-\frac{1}{R}\frac{\partial w}{\partial y}+\frac{\partial^2 w}{\partial y^2}\frac{\partial w}{\partial y})\\
&-B_{11}\frac{\partial^3 w}{\partial y^3}] + A_{31}^e\frac{\partial \phi}{\partial y}+A_{31}^m\frac{\partial \gamma}{\partial y} = 0
\end{aligned} \tag{66}$$

$$\begin{aligned}
&(1-l^2\nabla^2)[B_{11}(\frac{\partial^3 u}{\partial x^3}+\frac{\partial^3 w}{\partial x^3}\frac{\partial w}{\partial x}+\frac{\partial^2 w}{\partial x^2}\frac{\partial^2 w}{\partial x^2})\\
&-D_{11}\frac{\partial^4 w}{\partial x^4} - 2D_{12}\frac{\partial^4 w}{\partial x^2\partial y^2} - 4D_{66}\frac{\partial^4 w}{\partial x^2\partial y^2}
\end{aligned} \tag{67}$$

$$\begin{aligned}
&-D_{11}\frac{\partial^4 w}{\partial y^4}+B_{12}(\frac{\partial^3 v}{\partial x^2\partial y}-\frac{1}{R}\frac{\partial^2 w}{\partial x^2}+\frac{\partial^3 w}{\partial x^2\partial y}\frac{\partial w}{\partial y}\\
&+\frac{\partial^2 w}{\partial x\partial y}\frac{\partial^2 w}{\partial x\partial y}) + 2B_{66}(\frac{\partial^3 u}{\partial x\partial y^2}+\frac{\partial^3 v}{\partial x^2\partial y}\\
&+\frac{\partial^2 w}{\partial x^2}\frac{\partial^2 w}{\partial y^2}+\frac{\partial w}{\partial x}\frac{\partial^3 w}{\partial x\partial y^2}+\frac{\partial^3 w}{\partial x^2\partial y}\frac{\partial w}{\partial y}\\
&+\frac{\partial^2 w}{\partial x\partial y}\frac{\partial^2 w}{\partial x\partial y}) + B_{12}(\frac{\partial^3 u}{\partial x\partial y^2}+\frac{\partial w}{\partial x}\frac{\partial^3 w}{\partial x\partial y^2}\\
&+\frac{\partial^2 w}{\partial x\partial y}\frac{\partial^2 w}{\partial x\partial y}) + B_{11}(\frac{\partial^3 v}{\partial y^3}-\frac{1}{R}\frac{\partial^2 w}{\partial y^2}+\frac{\partial^3 w}{\partial y^3}\frac{\partial w}{\partial y}\\
&+\frac{\partial^2 w}{\partial y^2}\frac{\partial^2 w}{\partial y^2}) + \frac{A_{12}}{R}(\frac{\partial u}{\partial x}+\frac{1}{2}(\frac{\partial w}{\partial x})^2) - \frac{B_{12}}{R}\frac{\partial^2 w}{\partial x^2}\\
&+\frac{A_{11}}{R}(\frac{\partial v}{\partial y}-\frac{w}{R}+\frac{1}{2}(\frac{\partial w}{\partial y})^2) - \frac{B_{11}}{R}\frac{\partial^2 w}{\partial y^2}]\\
&+E_{31}^e(\frac{\partial^2 \phi}{\partial x^2}+\frac{\partial^2 \phi}{\partial y^2}) + E_{31}^m(\frac{\partial^2 \gamma}{\partial x^2}+\frac{\partial^2 \gamma}{\partial y^2})\\
&+\frac{A_{31}^e}{R}\phi+\frac{A_{31}^m}{R}\gamma+((1-l^2\nabla^2)[A_{11}(\frac{\partial u}{\partial x}+\frac{1}{2}(\frac{\partial w}{\partial x})^2)\\
&-B_{11}\frac{\partial^2 w}{\partial x^2}+A_{12}(\frac{\partial v}{\partial y}-\frac{w}{R}+\frac{1}{2}(\frac{\partial w}{\partial y})^2)\\
&-B_{12}\frac{\partial^2 w}{\partial y^2})] + A_{31}^e\phi+A_{31}^m\gamma)(\frac{\partial^2 w}{\partial x^2})\\
&+2(((1-l^2\nabla^2)[A_{66}(\frac{\partial u}{\partial y}+\frac{\partial v}{\partial x}+\frac{\partial w}{\partial x}\frac{\partial w}{\partial y})\\
&-2B_{66}\frac{\partial^2 w}{\partial x\partial y}])(\frac{\partial^2 w}{\partial x\partial y}) + (((1-l^2\nabla^2)[A_{12}(\frac{\partial u}{\partial x}+\frac{1}{2}(\frac{\partial w}{\partial x})^2)\\
&-B_{12}\frac{\partial^2 w}{\partial x^2}+A_{11}(\frac{\partial v}{\partial y}-\frac{w}{R}+\frac{1}{2}(\frac{\partial w}{\partial y})^2) - B_{11}\frac{\partial^2 w}{\partial y^2}]\\
&+A_{31}^e\phi+A_{31}^m\gamma)(\frac{\partial^2 w}{\partial y^2})\\
&+[-(N^E+N^H+N^M)(\frac{\partial^2 w}{\partial x^2}+\frac{\partial^2 w}{\partial y^2})] = 0
\end{aligned}$$

$$\begin{aligned}
&+F_{11}^e\frac{\partial^2 \phi}{\partial x^2}+F_{11}^m\frac{\partial^2 \gamma}{\partial x^2}+F_{22}^e\frac{\partial^2 \phi}{\partial y^2}+F_{22}^m\frac{\partial^2 \gamma}{\partial y^2}\\
&+A_{31}^e(\frac{\partial u}{\partial x}+\frac{1}{2}(\frac{\partial w}{\partial x})^2+\frac{\partial v}{\partial y}-\frac{w}{R}+\frac{1}{2}(\frac{\partial w}{\partial y})^2)\\
&-E_{31}^e(\frac{\partial^2 w}{\partial x^2}+\frac{\partial^2 w}{\partial y^2}) - F_{33}^e\phi - F_{33}^m\gamma = 0
\end{aligned} \tag{68}$$

$$\begin{aligned}
&+F_{11}^m\frac{\partial^2 \phi}{\partial x^2}+X_{11}^m\frac{\partial^2 \gamma}{\partial x^2}+F_{22}^m\frac{\partial^2 \phi}{\partial y^2}+X_{22}^m\frac{\partial^2 \gamma}{\partial y^2}\\
&+A_{31}^m(\frac{\partial u}{\partial x}+\frac{1}{2}(\frac{\partial w}{\partial x})^2+\frac{\partial v}{\partial y}-\frac{w}{R}+\frac{1}{2}(\frac{\partial w}{\partial y})^2)\\
&-E_{31}^m(\frac{\partial^2 w}{\partial x^2}+\frac{\partial^2 w}{\partial y^2}) - F_{33}^m\phi - X_{33}^m\gamma = 0
\end{aligned} \tag{69}$$

4. Solution by differential quadrature method (DQM)

In the present chapter, differential quadrature method (DQM) has been utilized for solving the governing equations for the MEE microshell. According to DQM, at an assumed grid point (x_i, y_j) the derivatives for function F are supposed as weighted linear summation of all functional values within the computation domains as:

$$\frac{d^n F}{dx^n}\Big|_{x=x_i} = \sum_{j=1}^{N} c_{ij}^{(n)} F(x_j) \tag{70}$$

where

$$C_{ij}^{(1)} = \frac{\pi(x_i)}{(x_i - x_j)\,\pi(x_j)} \qquad i,j = 1,2,\dots,N, \quad i \neq j \tag{71}$$

in which $\pi(x_i)$ is defined by

$$\pi(x_i) = \prod_{j=1}^{N} (x_i - x_j), \quad i \neq j \tag{72}$$

and when $i = j$

$$\begin{aligned} &C_{ij}^{(1)} = c_{ii}^{(1)} = -\sum_{k=1}^{N} C_{ik}^{(1)}, \\ &i = 1,2,\dots,N, \quad i \neq k, \qquad i = j \end{aligned} \tag{73}$$

Then, weighting coefficients for high orders derivatives may be expressed by:

$$\begin{aligned} C_{ij}^{(2)} &= \sum_{k=1}^{N} C_{ik}^{(1)} C_{kj}^{(1)} \\ C_{ij}^{(3)} &= \sum_{k=1}^{N} C_{ik}^{(1)} C_{kj}^{(2)} = \sum_{k=1}^{N} C_{ik}^{(2)} C_{kj}^{(1)} \\ C_{ij}^{(4)} &= \sum_{k=1}^{N} C_{ik}^{(1)} C_{kj}^{(3)} = \sum_{k=1}^{N} C_{ik}^{(3)} C_{kj}^{(1)} \qquad i,j = 1,2,\dots,N. \\ C_{ij}^{(5)} &= \sum_{k=1}^{N} C_{ik}^{(1)} C_{kj}^{(4)} = \sum_{k=1}^{N} C_{ik}^{(4)} C_{kj}^{(1)} \\ C_{ij}^{(6)} &= \sum_{k=1}^{N} C_{ik}^{(1)} C_{kj}^{(5)} = \sum_{k=1}^{N} C_{ik}^{(5)} C_{kj}^{(1)} \end{aligned} \tag{74}$$

According to presented approach, the dispersions of grid points based upon Gauss-Chebyshev-Lobatto assumption are expressed as:

$$\begin{aligned} x_i &= \frac{L}{2}\left[1 - \cos\left(\frac{i-1}{N-1}\pi\right)\right] \qquad i = 1,2,\dots,N, \\ y_j &= \pi R\left[1 - \cos\left(\frac{j-1}{M-1}\pi\right)\right] \qquad j = 1,2,\dots,M, \end{aligned} \tag{75}$$

Next, the displacement components may be re-written by

$$\{u, v, w, \phi, \gamma\}(x,y) = \{U, V, W, \Phi, \Upsilon\}(x,y) \tag{76}$$

where $\{U, V, W, \Phi, \Upsilon\}$ are the amplitudes. Then, it is possible to express obtained boundary conditions as:

$$\begin{aligned} &\phi = \gamma = w = 0, \\ &\frac{\partial^2 w}{\partial x^2} = \frac{\partial^2 w}{\partial y^2} = 0 \\ &\frac{\partial^4 w}{\partial x^4} = \frac{\partial^4 w}{\partial y^4} = 0 \end{aligned} \tag{77}$$

Now, one can express the modified weighting coefficients for all edges simply-supported as:

$$\begin{aligned} \bar{C}_{1,j}^{(2)} &= \bar{C}_{N,j}^{(2)} = 0, \qquad i = 1,2,\dots,M, \\ \bar{C}_{i,1}^{(2)} &= \bar{C}_{1,M}^{(2)} = 0, \qquad i = 1,2,\dots,N. \end{aligned} \tag{78}$$

and

$$\bar{C}_{ij}^{(3)} = \sum_{k=1}^{N} C_{ik}^{(1)} \bar{C}_{kj}^{(2)} \qquad \bar{C}_{ij}^{(4)} = \sum_{k=1}^{N} C_{ik}^{(1)} \bar{C}_{kj}^{(3)} \tag{79}$$

Considering DQ approach and placing displacement variables presented by Eq. (76) into Eqs. (65)-(69) yields the subsequent ordinary nonlinear governing equations as:

$$k_{11}U + k_{21}V + k_{31}W + n_1W^2 + k_{41}\Phi + k_{51}\Upsilon = 0 \tag{80}$$

$$k_{12}U + k_{22}V + k_{32}W + n_2W^2 + k_{42}\Phi + k_{52}\Upsilon = 0 \tag{81}$$

$$\begin{aligned} &k_{13}U + k_{23}V + k_{33}W + n_3W^2 + n_4W^3 + n_5UW \\ &+n_6VW + k_{43}\Phi + k_{53}\Upsilon + n_9\Phi W + n_{10}\Upsilon W = 0 \end{aligned} \tag{82}$$

$$k_{14}U + k_{24}V + k_{34}W + n_7W^2 + k_{44}\Phi + k_{54}\Upsilon = 0 \tag{83}$$

$$k_{15}U + k_{25}V + k_{35}W + n_8W^2 + k_{45}\Phi + k_{55}\Upsilon = 0 \tag{84}$$

in which n_i and k_{ij} express the components of non-linearity and linear stiffness matrices. Owning to the reason that five coupled nonlinear governing equations are available, providing the closed-form of critical force as a function of maximum amplitude (W) is very hard. Thus, by simultaneous solve of Eqs. (80)-(84), it is feasible to calculate amplitudes (U, V, Φ, Υ) as functions of transverse deflection or maximum deflection (W). Next, calculated amplitudes ($\hat{U}$, $\hat{V}$, $\hat{\Phi}$, $\hat{\Upsilon}$) have been placed in Eq. (82) in order to establish a single nonlinear equation for microshell as:

$$\begin{aligned} &k_{13}\hat{U} + k_{23}\hat{V} + k_{33}W + n_3W^2 + n_4W^3 + n_5\hat{U}W \\ &+n_6\hat{V}W + k_{43}\hat{\Phi} + k_{53}\hat{\Upsilon} + n_9\hat{\Phi}W + n_{10}\hat{\Upsilon}W = 0dz \end{aligned} \tag{85}$$

This equation must solved to obtain buckling loads as a function of W. Also, some normalized parameters may be presented in this article such as:

$$\begin{aligned} &\bar{N} = N^M \frac{L}{c_{11}^t h}, \lambda = \frac{l}{L}, \\ &\widehat{W} = W\delta\,, \delta = \frac{\pi^2 Rh}{L^2} \end{aligned} \tag{86}$$

5. Numerical results and discussions

By using differential quadrature method (DQM), a numerical investigation was provided for nonlinear stability behavior of magneto-electro-elastic (MEE) cylindrical shells at microscale. It is assumed that the cylindrical shell has been subjected to compressive loads leading to buckling phenomena in geometrically nonlinear regime. The non-uniformity of strain field has been inserted in the formulation for considering the microscale effects. The material properties of the shell are considered to be inhomogeneous with graded distribution where all properties are represented in Table 1.

Post-buckling load of a FG cylindrical shell obtained by presented study is compared with that provided by Bitch *et al*. (2013) as shown in Fig. 2. In this figure, a FG shell with material gradient indices p = 1, 5 and the length of L = 2R has been considered. Obtained buckling curves completely matches with that provided by Bich *et al*. (2013). Thus, the established formulation and solution technique is adequate for analysis of cylindrical shells.

Table 1 Material properties of the FG-METE shell

Properties	$BaTiO_3$	$CoFe_2O_4$
$c_{11} = c_{22}$ (GPa)	166	286
c_{12}	77	173
c_{66}	44.5	56.5
e_{31} (Cm^{-2})	-4.4	0
e_{15}	11.6	0
q_{31} (N/Am)	0	580.3
q_{15}	0	550
s_{11} ($10^{-9}C^2m^{-2}N^{-1}$)	11.2	0.08
s_{33}	12.6	0.093
$\chi_{11}(10^{-6}Ns^2C^{-2}/2)$	5	-590
χ_{33}	10	157
$d_{11} = d_{22} = d_{33}$	0	0
$\alpha_1(10^{-6}1/K)$	10	15.7

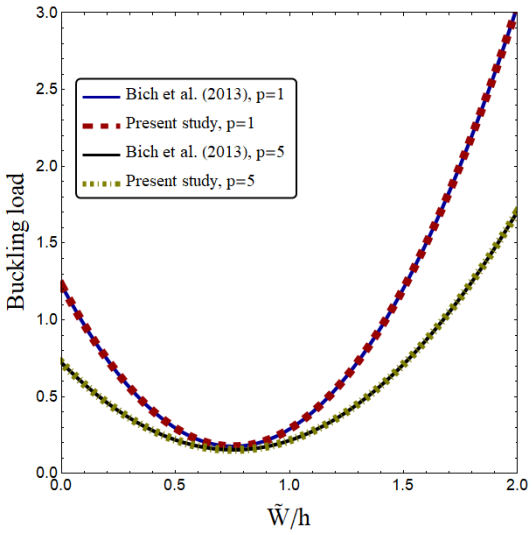

Fig. 2 Verification of post-buckling curves for FG shells

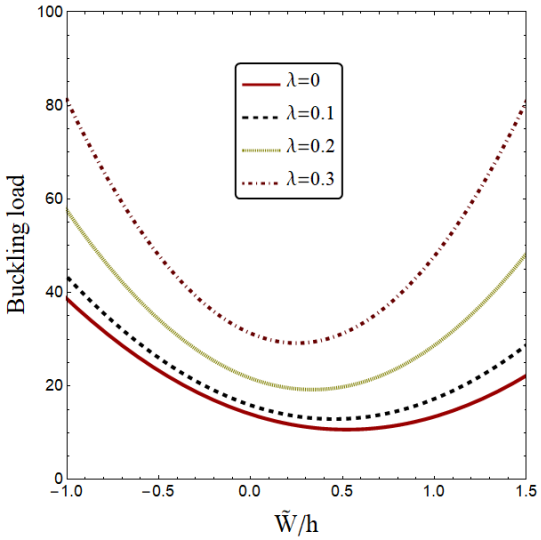

Fig. 3 Post-buckling load versus normalized deflection based on various strain gradient parameters (V = 0, Ω = 0, p = 1, h = 100 μm, L = 2R, R/h = 100)

Fig. 3 illustrates buckling load of FG-MEE microshell versus normalized deflection based on various strain gradient parameters when L = 2R and R/h = 100. For all curves, obtained buckling load at $\tilde{W}$ = 0 is called critical buckling load. With increase of normalized deflection in positive direction, post-buckling curves exhibit an interesting and surprising behavior. In fact, the buckling load of microshell first reduces with increase of normalized deflection then it increases. So, immediately after the critical buckling load, the microshell has no post-buckling capability and buckling load will reduce. It means that the microshell can be subjected to higher deformations under smaller loads. However, the buckling load will increase at higher normalized deflections where the microshell can endure higher loads. Another observation from this figure is that post-buckling curves of the microshell are influenced by strain gradient effects. Post-buckling curves move higher with increase of strain gradient parameter which introduces structural stiffening effect. In special cases when λ = 0, post-buckling curves of a macro size MEE shell can be obtained.

Influences of applied electric voltage (V) and material gradient index (p) on post-buckling curves of a FG-MEE microshell have been illustrated in Fig. 4 when λ = 0.2. It can be deduced that post-buckling curves of FG-MEE microshell rely on the value of material gradient index. Indeed, increase of material index yields lower post-buckling loads because the amount of $CoFe_2O_4$ having lower elastic moduli is decreased compared to the amount of $BaTiO_3$. Also, as the value of p is smaller, the post-buckling curves based on various values of applied electric voltage become closer to each other. It is due to the fact that at smaller values of p, the portion of $CoFe_2O_4$ in FG material is more than $BaTiO_3$. Since $CoFe_2O_4$ has a zero piezoelectric constant (e_{31} = 0) according to Table 1, electric field effects on post-buckling curves reduces at higher portion of $CoFe_2O_4$ or lower values of material index. Also, it may be observed from the figure that negative voltage gives higher post-buckling curves than positive voltage. Actually, positive voltage may induce an axial compressive load to the nanoshell leading to lower structural stiffness and buckling loads.

Fig. 5 indicates the effects of magnetic field intensity (Ω) on post-buckling curves of a FG-MEE microshell modeled by strain gradient theory. It may be seen from the figure that negative magnetic field intensity gives lower post-buckling curves than positive magnetic field intensity. Indeed, negative magnetic field intensity leads to lower structural stiffness by exerting an axial compressive load to the microshell.

From a scientific point of view, buckling occurs when the structures is subjected to a large compressive load. This load can be a mechanical load acting in axial direction leading to buckling of a microshell. Also, the microshell may buckle under an intense electric or magnetic field. The voltage in which the microshell buckles is called buckling voltage an. Fig. 6 depicts buckling voltage with respect to normalized maximum deflection and various values of strain gradient parameters. As can be seen, the microshell is buckled at positive values of electric voltage according to

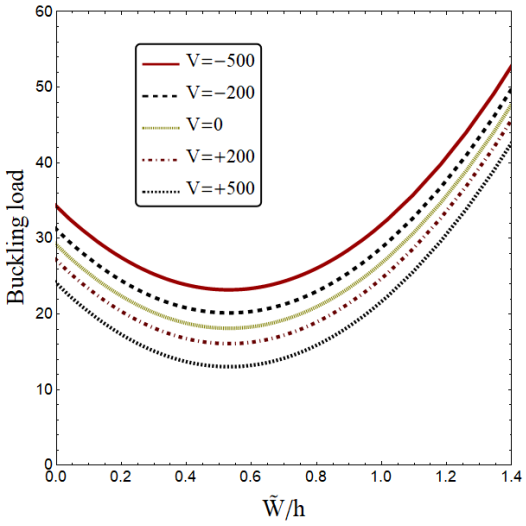

(a) p = 1

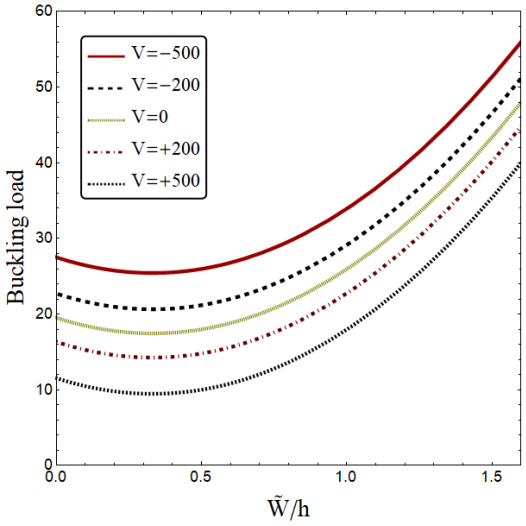

(b) p = 5

Fig. 4 Post-buckling load versus normalized deflection based on various electric voltages and material indices (Ω = 0, h = 1 μm, λ = 0.2, L = 2R, R/h = 100)

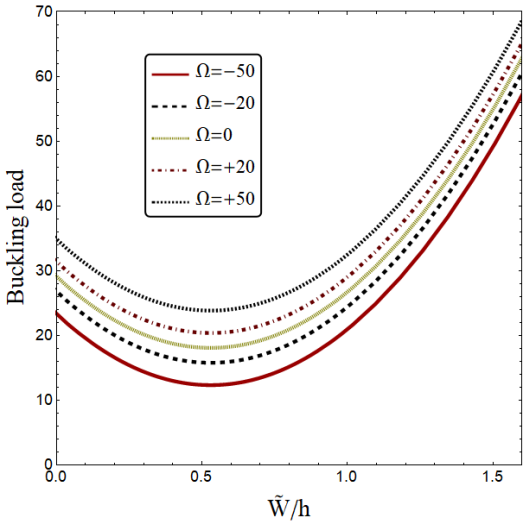

Fig. 5 Post-buckling load versus normalized deflection based on various electric magnetic field intensities (V = 0, h = 1 μm, λ = 0.2, L = 2R, R/h = 100)

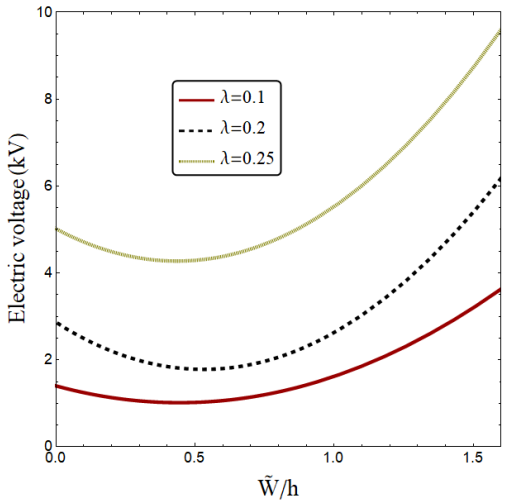

Fig. 6 Buckling voltage versus normalized deflection based on various electric voltages (Ω = 0, h = 1 μm, p = 1, L = 2R, R/h = 100)

Fig. 6. Considering absolute values of buckling voltage, the post-buckling curves first diminishes with increase of normalized deflection. Then, the post-buckling curves will rise at higher values of normalized deflection. As mentioned before, the cylindrical microshells have no post-buckling capability immediately after critical buckling values.

6. Conclusions

An investigation on post-buckling behavior of FG-MEE cylindrical microshell under mechanical, electrical and magnetic loadings was presented in the article. Mathematical formulation based on strain gradient theory gave a scale coefficient for the description of increase in structural stiffness at microscale. Functionally gradation of material properties was defined according to power-law function. The governing equations were presented in the framework of DQ method and then post-buckling curves were obtained as functions of maximum deflection. It was seen that the buckling load of microshell first reduced with increase of maximum deflection and then it increased. In fact, immediately after the critical buckling load, the microshell had no post-buckling capability and buckling load reduced. Another observation was that post-buckling curves of the microshell were influenced by strain gradient effects. It was also seen that increase of material index led to lower post-buckling loads. Also, as the value of material index was smaller, the post-buckling curves based on various values of applied electric voltage became closer to each other.

Acknowledgement

The work was supported by General scientific research projects of Wuhan Polytechnic University (2020Y11), This work was finished at Wuhan University of Technology (WUT) and Wuhan Polytechnic University, Wuhan.

References

Ahmed, R.A., Al-Maliki, A.F. and Faleh, N.M. (2020a), "Dynamic characteristics of multi-phase crystalline porous shells with using strain gradient elasticity", *Adv. Nano Res.*, **8**(2), 157-167. https://doi.org/10.12989/anr.2020.8.2.157.

Ahmed, R.A., Mustafa, N.M., Faleh, N.M. and Fenjan, R.M. (2020b), "Nonlocal nonlinear stability of higher-order porous beams via Chebyshev-Ritz method", *Struct. Eng. Mech.*, **76**(3), 413-420. https://doi.org/10.12989/sem.2020.76.3.413.

Ahmed, R.A., Fenjan, R.M., Hamad, L.B. and Faleh, N.M. (2020c), "A review of effects of partial dynamic loading on dynamic response of nonlocal functionally graded material beams", *Adv. Mater. Res.*, **9**(1), 33-48. https://doi.org/10.12989/amr.2020.9.1.033.

Arefi, M., Kiani, M. and Rabczuk, T. (2019), "Application of nonlocal strain gradient theory to size dependent bending analysis of a sandwich porous nanoplate integrated with piezomagnetic face-sheets", *Compos. Part B Eng.*, **168**, 320-333. https://doi.org/10.1016/j.compositesb.2019.02.057.

Aydogdu, M., Arda, M. and Filiz, S. (2018), "Vibration of axially functionally graded nano rods and beams with a variable nonlocal parameter", *Adv. Nano Res.*, **6**(3), 257-278. https://doi.org/10.12989/anr.2018.6.3.257.

Barati, M.R. and Zenkour, A.M. (2018), "Electro-thermoelastic vibration of plates made of porous functionally graded piezoelectric materials under various boundary conditions", *J. Vib. Control*, **24**(10), 1910-1926. https://doi.org/10.1177%2F1077546316672788.

Barati, M.R. and Shahverdi, H. (2021), "Assessment of nonlinear vibrations of thin plates undergoing large deflection and moderate rotation using Jacobi elliptic functions", *Mech. Based Des. Struct.*, 1-17. https://doi.org/10.1080/15397734.2021.1956329.

Barretta, R., Feo, L., Luciano, R., de Sciarra, F.M. and Penna, R. (2016), "Functionally graded Timoshenko nanobeams: A novel nonlocal gradient formulation", *Compos. Part B Eng.*, **100**, 208-219. https://doi.org/10.1016/j.compositesb.2016.05.052.

Bich, D.H., Nguyen, N.X. and Van Tung, H. (2013), "Postbuckling of functionally graded cylindrical shells based on improved Donnell equations", *Vietnam J. Mech.*, **35**(1), 1-15. https://doi.org/10.15625/0866-7136/35/1/2894.

Chen, C., Wang, X., Wang, Y., Yang, D., Yao, F., Zhang, W. and Hu, D. (2020), "Additive manufacturing of piezoelectric materials", *Adv. Funct. Mater.*, **30**(52), 2005141. https://doi.org/10.1002/adfm.202005141.

Chikh, A., Bakora, A., Heireche, H., Houari, M.S.A., Tounsi, A. and Bedia, E.A. (2016), "Thermo-mechanical postbuckling of symmetric S-FGM plates resting on Pasternak elastic foundations using hyperbolic shear deformation theory", *Struct. Eng. Mech.*, **57**(4), 617-639. https://doi.org/10.12989/sem.2016.57.4.617.

Dai, Z., Xie, J., Fan, X., Ding, X., Liu, W., Zhou, S. and Ren, X. (2020), "Enhanced energy storage properties and stability of Sr($Sc_{0.5}Nb_{0.5}$)O_3 modified 0.65$BaTiO_3$-0.35$Bi_{0.5}Na_{0.5}TiO$ ceramics", *Chem. Eng. J.*, **397**, 125520. https://doi.org/10.1016/j.cej.2020.125520.

Dai, Z., Guo, S., Gong, Y. and Wang, Z. (2021a), "Semiconductor flexoelectricity in graphite-doped SrTiO3 ceramics", *Ceram. Int.*, **47**(5), 6535-6539. https://doi.org/10.1016/j.ceramint.2020.10.239.

Dai, Z., Xie, J., Chen, Z., Zhou, S., Liu, J., Liu, W. and Ren, X. (2021b), "Improved energy storage density and efficiency of (1−x)$Ba_{0.85}Ca_{0.15}Zr_{0.1}Ti_{0.9}O_3$-x$BiMg_{2/3}NbO_3$ lead-free ceramics", *Chem. Eng. J.*, **410**, 128341. https://doi.org/10.1016/j.cej.2020.128341.

Ebrahimi, F. and Barati, M.R. (2019a), "Hygrothermal effects on static stability of embedded single-layer graphene sheets based on nonlocal strain gradient elasticity theory", *J. Therm. Stresses*, **42**(12), 1535-1550. https://doi.org/10.1080/01495739.2019.1662352.

Ebrahimi, F. and Barati, M.R. (2019b), "On static stability of electro-magnetically affected smart magneto-electro-elastic nanoplates", *Adv. Nano Res.*, **7**(1), 63-75. http://doi.org/10.12989/anr.2019.7.1.063.

Ebrahimi, F. and Barati, M.R. (2019c), "Dynamic modeling of embedded nanoplate systems incorporating flexoelectricity and surface effects", *Microsyst. Technol.*, **25**(1), 175-187. https://doi.org/10.1007/s00542-018-3946-7.

Eltaher, M.A., Khater, M.E. and Emam, S.A. (2016), "A review on nonlocal elastic models for bending, buckling, vibrations, and wave propagation of nanoscale beams", *Appl. Math. Model.*, **40**(5-6), 4109-4128. https://doi.org/10.1016/j.apm.2015.11.026.

Eringen, A.C. (1983), "On differential equations of nonlocal elasticity and solutions of screw dislocation and surface waves", *J. Appl. Phys.*, **54**(9), 4703-4710. https://doi.org/10.1063/1.332803.

Fang, J., Liu, C., Simos, T.E. and Famelis, I.T. (2020), "Neural network solution of single-delay differential equations", *Mediterranean J. Math.*, **17**(1), 1-15. https://doi.org/10.1007/s00009-019-1452-5.

Farajpour, A., Yazdi, M.H., Rastgoo, A., Loghmani, M. and Mohammadi, M. (2016), "Nonlocal nonlinear plate model for large amplitude vibration of magneto-electro-elastic nanoplates", *Compos. Struct.*, **140**, 323-336. https://doi.org/10.1016/j.compstruct.2015.12.039.

Fenjan, R.M., Ahmed, R.A. and Faleh, N.M. (2021), "Post-buckling analysis of imperfect nonlocal piezoelectric beams under magnetic field and thermal loading", *Struct. Eng. Mech.*, **78**(1), 15-22. https://doi.org/10.12989/sem.2021.78.1.015.

Heydarpour, Y. and Malekzadeh, P. (2019), "Dynamic stability of cylindrical nanoshells under combined static and periodic axial loads", *J. Brazil. Soc. Mech. Sci. Eng.*, **41**(4), 184. https://doi.org/10.1007/s40430-019-1675-1.

Ke, L.L. and Wang, Y. S. (2014), "Free vibration of size-dependent magneto-electro-elastic nanobeams based on the nonlocal theory", *Physica E*, **63**, 52-61. https://doi.org/10.1016/j.physe.2014.05.002.

Ke, L.L., Wang, Y.S., Yang, J. and Kitipornchai, S. (2014), "The size-dependent vibration of embedded magneto-electro-elastic cylindrical nanoshells", *Smart Mater. Struct.*, **23**(12), 125036. https://doi.org/10.1088/0964-1726/23/12/125036.

Kovalnogov, V.N., Simos, T.E., and Tsitouras, C. (2020), "Ninth-order, explicit, two-step methods for second-order inhomogeneous linear IVPs", *Math. Method Appl. Sci.*, **43**(7), 4918-4926. https://doi.org/10.1002/mma.6246.

Li, L. and Hu, Y. (2015), "Buckling analysis of size-dependent nonlinear beams based on a nonlocal strain gradient theory", *Int. J. Eng. Sci.*, **97**, 84-94. https://doi.org/10.1016/j.ijengsci.2015.08.013.

Li, L. and Hu, Y. (2016), "Nonlinear bending and free vibration analyses of nonlocal strain gradient beams made of functionally graded material", *Int. J. Eng. Sci.*, **107**, 77-97. https://doi.org/10.1016/j.ijengsci.2016.07.011.

Li, T., Dai, Z., Yu, M. and Zhang, W. (2021), "Numerical investigation on the aerodynamic resistances of double-unit trains with different gap lengths", *Eng. Appl. Comput. Fluid Mech.*, **15**(1), 549-560. https://doi.org/10.1080/19942060.2021.1895321.

Lu, L., Guo, X. and Zhao, J. (2017), "Size-dependent vibration analysis of nanobeams based on the nonlocal strain gradient theory", *Int. J. Eng. Sci.*, **116**, 12-24. https://doi.org/10.1016/j.ijengsci.2017.03.006.

Ma, L.H., Ke, L.L., Reddy, J.N., Yang, J., Kitipornchai, S. and

Wang, Y.S. (2018), "Wave propagation characteristics in magneto-electro-elastic nanoshells using nonlocal strain gradient theory", *Compos. Struct.*, **199**, 10-23. https://doi.org/10.1016/j.compstruct.2018.05.061.

Mehralian, F., Beni, Y.T. and Zeverdejani, M.K. (2017a), "Calibration of nonlocal strain gradient shell model for buckling analysis of nanotubes using molecular dynamics simulations", *Physica B*, **521**, 102-111. https://doi.org/10.1016/j.physb.2017.06.058.

Mehralian, F., Beni, Y.T. and Zeverdejani, M.K. (2017b), "Nonlocal strain gradient theory calibration using molecular dynamics simulation based on small scale vibration of nanotubes", *Physica B*, **514**, 61-69. https://doi.org/10.1016/j.physb.2017.03.030.

Medvedev, M.A., Simos, T.E. and Tsitouras, C. (2020), "Explicit, Eighth-Order, Four-Step Methods for Solving y″= *f*(*x*,*y*)", *Bull. Malaysian Math. Sci. Soc.*, **43**(5), 3791-3807. https://doi.org/10.1007/s40840-019-00879-6.

Medvedeva, M.A., Simos, T.E. and Tsitouras, C. (2021a), "Sixth-order, P-stable, Numerov-type methods for use at moderate accuracies", *Math. Method. Appl. Sci.*, **44**(8), 6923-6930. https://doi.org/10.1002/mma.7233.

Medvedeva, M.A., Simos, T.E. and Tsitouras, C. (2021b), "Exponential integrators for linear inhomogeneous problems", *Math. Method. Appl. Sci.*, **44**(1), 937-944. https://doi.org/10.1002/mma.6802.

Mirjavadi, S.S., Forsat, M., Badnava, S., Barati, M.R. and Hamouda, A.M.S. (2020a), "Nonlinear dynamic characteristics of nonlocal multi-phase magneto-electro-elastic nano-tubes with different piezoelectric constituents", *Appl. Phys. A*, **126**(8), 1-16. https://doi.org/10.1007/s00339-020-03743-8.

Mirjavadi, S.S., Yahya, Y.Z., Forsat, M., Khan, I., Hamouda, A.M. S. and Barati, M.R. (2020b), "Magneto-electric effects on nonlocal nonlinear dynamic characteristics of imperfect multi-phase magneto-electro-elastic beams", *J. Magnetism. Magnet. Mater.*, **503**, 166649. https://doi.org/10.1016/j.jmmm.2020.166649.

Mirjavadi, S.S., Bayani, H., Khoshtinat, N., Forsat, M., Barati, M. R. and Hamouda, A.M.S. (2020c), "On nonlinear vibration behavior of piezo-magnetic doubly-curved nanoshells", *Smart Struct. Syst.*, **26**(5), 631-640. https://doi.org/10.12989/sss.2020.26.5.631.

Mirjavadi, S.S., Nikookar, M., Mollaee, S., Forsat, M., Barati, M. R. and Hamouda, A.M.S. (2020d), "Analyzing exact nonlinear forced vibrations of two-phase magneto-electro-elastic nanobeams under an elliptic-type force", *Adv. Nano Res.*, **9**(1), 47-58. https://doi.org/10.12989/anr.2020.9.1.047.

Mirjavadi, S.S., Forsat, M., Yahya, Y.Z., Barati, M.R., Jayasimha, A.N. and Hamouda, A.M.S. (2020e), "Porosity effects on post-buckling behavior of geometrically imperfect metal foam doubly-curved shells with stiffeners", *Struct. Eng. Mech.*, **75**(6), 701-711. https://doi.org/10.12989/sem.2020.75.6.701.

Mirjavadi, S.S., Forsat, M., Barati, M.R. and Hamouda, A.M.S. (2020g), "Assessment of transient vibrations of graphene oxide reinforced plates under pulse loads using finite strip method", *Comput. Concrete*, **25**(6), 575-585. https://doi.org/10.12989/cac.2020.25.6.575.

Mirjavadi, S.S., Forsat, M., Yahya, Y.Z., Barati, M.R., Jayasimha, A.N. and Khan, I. (2020h), "Analysis of post-buckling of higher-order graphene oxide reinforced concrete plates with geometrical imperfection", *Adv. Concrete Constr.*, **9**(4), 397-406. https://doi.org/10.12989/acc.2020.9.4.397.

Muhammad, A.K., Hamad, L.B., Fenjan, R.M. and Faleh, N.M. (2019), "Analyzing large-amplitude vibration of nonlocal beams made of different piezo-electric materials in thermal environment", *Adv. Mater. Res.*, **8**(3), 237-257. https://doi.org/10.12989/amr.2019.8.3.237.

Pan, E. (2001), "Exact solution for simply supported and multilayered magneto-electro-elastic plates", *J. Appl. Mech.*, **68**(4), 608-618. https://doi.org/10.1115/1.1380385.

Qiao, Y.X., Sheng, S.L., Zhang, L.M., Chen, J., Yang, L.L., Zhou, H.L. and Zheng, Z.B. (2021), "Friction and wear behaviors of a high nitrogen austenitic stainless steel Fe-19Cr-15Mn-0.66 N". *J. Min. Metall*, **57**(2), 285-293. https://doi.org/10.2298/JMMB201026025Q.

Ramirez, F., Heyliger, P.R. and Pan, E. (2006), "Free vibration response of two-dimensional magneto-electro-elastic laminated plates", *J. Sound Vib.*, **292**(3-5), 626-644. https://doi.org/10.1016/j.jsv.2005.08.004.

Sayyad, A.S. and Ghugal, Y.M. (2018), "An inverse hyperbolic theory for FG beams resting on Winkler-Pasternak elastic foundation", *Adv. Aircraft Spacecraft Sci.*, **5**(6), 671-689. https://doi.org/10.12989/aas.2018.5.6.671.

Shariati, A., Barati, M.R., Ebrahimi, F. and Toghroli, A. (2020a), "Investigation of microstructure and surface effects on vibrational characteristics of nanobeams based on nonlocal couple stress theory", *Adv. Nano Res.*, **8**(3), 191-202. https://doi.org/10.12989/anr.2020.8.3.191.

Shariati, A., Barati, M.R., Ebrahimi, F., Singhal, A. and Toghroli, A. (2020b), "Investigating vibrational behavior of graphene sheets under linearly varying in-plane bending load based on the nonlocal strain gradient theory", *Adv Nano Res.*, **8**(4), 265-276. https://doi.org/10.12989/anr.2020.8.4.265.

She, G.L., Yuan, F.G., Ren, Y.R., Liu, H.B. and Xiao, W.S. (2018), "Nonlinear bending and vibration analysis of functionally graded porous tubes via a nonlocal strain gradient theory", *Compos. Struct.*, **203**, 614-623. https://doi.org/10.1016/j.compstruct.2018.07.063.

Şimşek, M. (2019), "Some closed-form solutions for static, buckling, free and forced vibration of functionally graded (FG) nanobeams using nonlocal strain gradient theory", *Compos. Struct.*, **224**, 111041. https://doi.org/10.1016/j.compstruct.2019.111041.

Simos, T.E. and Tsitouras, C. (2020), "Explicit, ninth order, two step methods for solving inhomogeneous linear problems $x''(t) = \Lambda x(t) + f(t)$", *Appl. Numer. Math.*, **153**, 344-351. https://doi.org/10.1016/j.apnum.2020.03.003.

Simos, T.E. and Tsitouras, C. (2021), "Evolutionary derivation of Runge–Kutta pairs for addressing inhomogeneous linear problems", *Numer. Algorithms*, **87**(2), 511-525. https://doi.org/10.1007/s11075-020-00976-9.

Sun, J., Aslani, F., Wei, J. and Wang, X. (2021), "Electromagnetic absorption of copper fiber oriented composite using 3D printing", *Constr. Build. Mater.*, **300**, 124026. https://doi.org/10.1016/j.conbuildmat.2021.124026.

Tan, L., Sun, Y., Wei, C., Tao, Y., Tian, Y., An, Y. and Feng, J. (2021), "Design of robust, lithiophilic, and flexible inorganic-polymer protective layer by separator engineering enables dendrite-free lithium metal batteries with $LiNi_{0.8}Mn_{0.1}Co_{0.1}O_2$ cathode", *Small*, **17**(13), 2007717. https://doi.org/10.1002/smll.202007717.

Uzun, B. and Civalek, Ö. (2019), "Free vibration analysis Silicon nanowires surrounded by elastic matrix by nonlocal finite element method", *Adv. Nano Res.*, **7**(2), 99-108. https://doi.org/10.12989/anr.2019.7.2.099.

Waksmanski, N. and Pan, E. (2017), "An analytical three-dimensional solution for free vibration of a magneto-electro-elastic plate considering the nonlocal effect", *J. Intell. Mater. Syst. Struct.*, **28**(11), 1501-1513. https://doi.org/10.1177%2F1045389X16672734.

Xu, X. and Nieto-Vesperinas, M. (2019), "Azimuthal imaginary Poynting momentum density", *Phys. Rev. Lett.*, **123**(23), 233902. https://doi.org/10.1103/PhysRevLett.123.233902.

Yan, D., Wang, W. and Chen, Q. (2020), "Fractional-order

modeling and nonlinear dynamic analyses of the rotor-bearing-seal system", *Chaos Soliton Fract.*, **133**, 109640. https://doi.org/10.1016/j.chaos.2020.109640.

Zeighampour, H., Beni, Y.T. and Dehkordi, M.B. (2018), "Wave propagation in viscoelastic thin cylindrical nanoshell resting on a visco-Pasternak foundation based on nonlocal strain gradient theory", *Thin Wall. Struct.*, **122**, 378-386. https://doi.org/10.1016/j.tws.2017.10.037.

Zhang, C. and Ou, J. (2015), "Modeling and dynamical performance of the electromagnetic mass driver system for structural vibration control", *Eng. Struct.*, **82**, 93-103. https://doi.org/10.1016/j.engstruct.2014.10.029.

Zhang, X. and Zhang, Y. (2021a), "Experimental study on enhanced heat transfer and flow performance of magnetic nanofluids under alternating magnetic field. International journal of thermal sciences", **164**, 106897. https://doi.org/10.1016/j.ijthermalsci.2021.106897.

Zhang, X. and Zhang, Y. (2021b), "Heat transfer and flow characteristics of Fe3O4-water nanofluids under magnetic excitation", *Int. J. Therm. Sci.*, **163**, 106826. https://doi.org/10.1016/j.ijthermalsci.2020.106826.

Zhao, X., Zhu, W.D. and Li, Y.H. (2020a), "Analytical solutions of nonlocal coupled thermoelastic forced vibrations of micro-/nano-beams by means of Green's functions", *J. Sound Vib.*, **481**, 115407. https://doi.org/10.1016/j.jsv.2020.115407.

Zhao, N., Deng, L., Luo, D. and Zhang, P. (2020b), "One-step fabrication of biomass-derived hierarchically porous carbon/MnO nanosheets composites for symmetric hybrid supercapacitor", *Appl. Surf. Sci.*, **526**, 146696. https://doi.org/10.1016/j.apsusc.2020.146696.

Zhu, W., Deng, M., Chen, D., Zhang, Z., Chai, W., Chen, D. and Hao, Y. (2020), "Dual-phase $CsPbCl_3$–Cs_4PbCl_6 perovskite films for self-powered, visible-blind UV photodetectors with fast response", *ACS Appl. Mater. Interfac.*, **12**(29), 32961-32969. https://doi.org/10.1021/acsami.0c09910.

CC